Title

Pathoarchitectonics of the cerebral cortex in chorea-acanthocytosis and Huntington's disease

Journal

Neuropathology and Applied Neurobiology, 45(3)

ISSN

0305-1846

Authors

Liu, J
Heinsen, H
Grinberg, LT
et al.

Publication Date

2019-04-01

DOI

10.1111/nan.12495

Peer reviewed

HHS Public Access

Author manuscript

Neuropathol Appl Neurobiol. Author manuscript; available in PMC 2020 April 01.

Published in final edited form as:

Neuropathol Appl Neurobiol. 2019 April ; 45(3): 230–243. doi:10.1111/nan.12495.

Pathoarchitectonics of the cerebral cortex in chorea-acanthocytosis and Huntington's disease

J. Liu[*,†], **H. Heinsen**[‡,§], **L. T. Grinberg**[¶], **E. Alho**[**], **E. Amaro Jr**[††], **C. A. Pasqualucci**[§], **U. Rüb**[‡‡,1], **K. Seidel**[‡‡,§§], **W. den Dunnen**[¶¶], **T. Arzberger**[***,†††], **C. Schmitz**[‡‡‡], **M. C. Kiessling**[‡‡‡], **B. Bader**[†,§§§], **A. Danek**[†]

[*]Department of Neurology, Xuanwu Hospital, Capital Medical University, Beijing, China, [†]Neurologische Klinik und Poliklinik, Ludwig-Maximilians-Universität München, München, [‡]Department of Psychiatry, Psychosomatics and Psychotherapy, Center of Mental Health, University Hospital Würzburg, Würzburg, Germany, [§]Ageing Brain Study Group, Department of Pathology, University of São Paulo Medical School, São Paulo, Brazil, [¶]Department of Neurology, University of California, San Francisco, San Francisco, CA, USA, [**]Praça Amadeu Amaral, University of São Paulo Medical School, São Paulo, Brazil, [††]Department of Radiology, University of São Paulo Medical School, São Paulo, Brazil, [‡‡]Experimental Neurobiology (Anatomical Institute II), Goethe-University, Frankfurt/Main, [§§]Anatomy & Cell Biology, Medical Faculty, Anatomical Institute, University of Bonn, Bonn, Germany, [¶¶]Department of Pathology and Medical Biology, University Medical Center Groningen University of Groningen, Groningen, The Netherlands, [***]Center for Neuropathology and Prion Research, Ludwig-Maximilians-Universität München, Munich, Germany [†††]Department of Psychiatry and Psychotherapy, Ludwig-Maximilians-Universität München, Munich, Germany [‡‡‡]Department of Neuroanatomy, Ludwig-Maximilians-Universität München, Munich, Germany [§§§]Clienia Privatklinik für Psychiatrie und Psychotherapie, Oetwil am See, Switzerland

Abstract

Aims: Quantitative estimation of cortical neurone loss in cases with chorea-acanthocytosis (ChAc) and its impact on laminar composition.

Methods: We used unbiased stereological tools to estimate the degree of cortical pathology in serial gallocyanin-stained brain sections through the complete hemispheres of three subjects with genetically verified ChAc and a range of disease durations. We compared these results with our previous data of five Huntington's disease (HD) and five control cases. Pathoarchitectonic changes

Correspondence: Helmut Heinsen, Department of Psychiatry, Psychosomatics and Psychotherapy, Center of Mental Health, University Hospital Würzburg, Germany. Tel: +55 11 988 311 039; heinsen@mail.uni-wuerzburg.de.

[1]Prof. Dr. Udo Rüb passed away 29th of June 2017. We mourn him as our colleague, friend and passionate researcher in the field of neurodegenerative diseases.

Author contributions

H.H., A.D. and B.B. conceived and designed the study; J.L., H.H., L.T.G., E.A., E.A. Jr, C.A.P., U.R., K.S., W.D., T.A., C.S. and M.K. acquired and analysed the data; H.H., J.L., and M.K. drafted the manuscript and figures.

Conflict of interest

The authors have no conflict of interest with regard to the contents of this study.

were exemplarily documented in TE1 of a 61-year-old female HD-, a 60-year-old female control case, and ChAc3.

Results: Macroscopically, the cortical volume of our ChAc cases (ChAc1–3) remained close to normal. However, the average number of neurones was reduced by 46% in ChAc and by 33% in HD ($P = 0.03$ for ChAc & HD *vs.* controls; $P = 0.64$ for ChAc *vs.* HD). Terminal HD cases featured selective laminar neurone loss with pallor of layers III, V and VIa, a high density of small, pale, closely packed radial fibres in deep cortical layers VI and V, shrinkage, and chromophilia of subcortical white matter. In ChAc, pronounced diffuse astrogliosis blurred the laminar borders, thus masking the complete and partial loss of pyramidal cells in layer IIIc and of neurones in layers III, V and VI.

Conclusion: ChAc is a neurodegenerative disease with distinct cortical neurodegeneration. The hypertrophy of the peripheral neuropil space of minicolumns with coarse vertical striation was characteristic of ChAc. The role of astroglia in the pathogenesis of this disorder remains to be elucidated.

Keywords

minicolumn; neurodegenerative disease; neurone number; selective vulnerability; stereology

Introduction

Chorea-acanthocytosis (ChAc) is one of the core neuroacanthocytosis syndromes [1]. It is caused by mutations in the vacuolar protein sorting 13 homolog A (*VPS13A*) gene (spanning a region of about 250 kb on chromosome 9 and comprising 73 exons) and is transmitted as an autosomal recessive trait [2–4]. More than 70 different *VPS13A* mutations have been described to date. Most of these result in the absence of chorein, the protein encoded by *VPS13A*. Chorein consists of 3174 amino acids and is expressed ubiquitously, although its function remains unknown.

Less than one thousand individuals worldwide have been diagnosed with ChAc. To date, a limited number of post-mortem studies of brains from these patients have been published [5–16]. Most of these investigations were conducted before the advent of genetic testing and erroneous diagnoses are, therefore, possible. These previous studies identified striking neuropathological similarities between ChAc and Huntington's disease (HD). A hallmark of both diseases is the severe degeneration of the caudate nucleus and putamen associated with marked astrogliosis, in some cases the pallidum and the reticulate part of the subtstantia nigra are also involved, and a mild to moderate gliosis in the thalamus was described [17,18]. The cortex appeared more or less spared in ChAc. [5–16]. Whereas ChAc is caused by a loss of chorein function, HD arises from a toxic gain of function due to the accumulation of extended polyglutamine tracts in the huntingtin protein. Therefore, even though these two conditions share some clinical symptoms, it would be surprising if they showed identical neuropathological features.

In order to investigate the spectrum of cortical pathology in ChAc, we used unbiased stereology to analyse the brains of three subjects with genetically confirmed ChAc. We then

compared our quantitative findings to previous quantitative data generated during a study of five HD patients and five age- and gender-matched control individuals [19]. Finally, we correlated our quantitative results with pathoarchitectonic studies on a polymodal isocortex lining the banks of the superior temporal sulcus. This corresponded to Brodmann's areas 21 and 22 [20], and von Economo-Koskinas [21] area temporalis propria (TE1).

Materials and methods

Brain specimens

Cerebral hemispheres from three patients with genetically confirmed ChAc (Table 1) were sourced from the Advocacy for Neuroacanthocytosis Patients for deposition in the Center for Neuropathology and Prion Research at the University of Munich. The analysis of human tissue in this study was approved by the ethical committees of the Goethe University in Frankfurt, Ludwig-Maximilians-University of Munich, the Julius-Maximilians-University of Würzburg and the Universidade de São Paulo.

For comparison, we used quantitative data from five HD cases that had been analysed previously using similar techniques [19]. At the time of HD tissue procurement, genetic testing for CAG-repeats was not available. The brains were donated from cases, who were in most instances hospitalized for one or two decades in two state psychiatric hospitals in southern and southwestern parts of Germany and whose family histories of probable HD were verified from their next of kins living in a radius of about 75 km from the psychiatric clinics and who were interested in the diagnoses. In the absence of genetic testing, other diseases with similar clinical symptoms including SCA17 [22] and HDL-2 cannot completely be excluded. SCA17 is a very rare disease in Germany. Fifteen patients from four families living in the north-western part of Germany, hundreds of kilometres away from the region our patients were born, were described by Schöls *et al.* None of them were diagnosed with HD [23]. HDL-2 is confined to Africans [24]. Vonsattel grading of striatal atrophy was not performed in the five HD cases.

Tissue processing and celloidin mounting

After procurement, the brainstem (with the cerebellum) was separated from the forebrain at the level of the rostral pons, and the hemispheres were severed mediosagittally. Fixation and tissue processing were performed under identical conditions for all brains. Either the right or left hemisphere, or the complete brain, were immersion-fixed in 20% formalin for at least 3 months, and then dehydrated in graded concentrations of ethanol. After dehydration, the hemispheres or complete brain were celloidin-embedded under a slight vacuum of about 100 mbar. Details of this procedure have been described previously [25]. The celloidin blocks were cut into serial 420 μm-thick coronal sections using a sliding microtome (Polycut, Leica Mikrosysteme Vertrieb GmbH Wetzlar, Germany). Every second section was stained with gallocyanin, a Nissl stain [26].

Design-based stereological analyses

Design-based stereological analyses were performed using a stereology workstation comprised of a Zeiss Axioplan II microscope (Carl Zeiss MicroImaging, Thornwood, NY,

USA) equipped with Plan-Neofluar 2.5× (N.A. = 0.075) and 40× (N.A. = 1.30) objectives, Fluar 10× (N.A. = 0.5) and 20× (N.A. = 0.75) objectives, a Microfire CCD camera (Optronics, Goleta, CA, USA), a motorized stage (Ludl Electronics, Hawthorne, NY, USA), and stereology software (StereoInvestigator, Version 10; MBF Bioscience, Williston, VT, USA).

The outlines of the cerebral cortex were manually traced in every 10th serial section (33–38 sections per hemisphere) by following with a cursor the cortical boundaries displayed on the video screen of the stereology workstation. Within these projection areas cortical volumes were calculated using Cavalieri's principle, by measuring the projection area of the regions on all sections, and multiplying it by the interval of the selected sections, and by the thickness of the sections [27]. The StereoInvestigator software generated counting grids and unbiased counting frames in a systematic-random fashion throughout the delineated regions. The total neurone number was evaluated using the optical fractionator probe [28]. The counting frame was 70 × 70 μm. The dissector height was set at 25 μm and the guard zone at 10 μm. All cells whose nuclear boundaries or (if present) nucleoli came into focus across the dissector height were counted. Finally, the cell density was calculated by dividing the total cell number by the volume of the region. Manual cell detection was used because current automated 3D cell detection methods were not appropriate for this study [29]. Estimation of cortical neurone density can be cumbersome even in control cases. The majority of Nissl-stained neurones featured relatively big nuclei enclosing one nucleolus (at least in humans) and their basophilic cytoplasm, frequently with a characteristic form (pyramidal, spindle-shaped) that contains Nissl-bodies. About 20% of neurones were smaller, granule cells were very small and a nucleolus could not always be identified by light microscopy. Although their nuclei can be confused with astrocytes, a small rim of basophilic cytoplasm surrounds the granule cells only, facilitating recognition. Granule cells in the frontal cortex tended to be more pyramidal or polygonal, whereas those of the parietal and occipital lobes were round to oval [21,30]. To reduce the burden of time invested in cell counting, we have classified equivocal granule cells as unidentified cortical cells. Normal astroglial cells were characterized by small round to oval light nuclei, the absence of nucleoli, and a cytoplasm that remains unstained with Nissl-stains. However, the nuclei of reactive astrocytes were increased in size enclosing a nucleolus or bigger heterochromatin granules mimicking nucleoli. A faintly stained cytoplasm may be identified which can contain numerous fine lipofuscin granules. Nuclei of oligodendrocytes were smaller than those of astrocytes, round, containing densely packed heterochromatin granules.

At variance with the present protocol we had estimated the cortical and striatal volume of our HD cases by point counting [19]. Prior to a comprehensive post-mortem study on the neurone number of five subcortical regions in 13 patients with schizophrenia and 13 age- and sex matched controls [27], we made a pilot study between two researchers engaged with counting since striatal neurone number had been estimated by HH with point counting and disectors whereas PK had used a StereoInvestigator for analysis of the other four subcortical nuclei. The results were similar and did not differ statistically. When analysing a low number of cases [31–35], it is indispensable to count a high number of nuclear profiles in order to enhance the precision of counting. We had counted at least 1000 profiles for the

study in schizophrenics and controls and more than 2000 profiles of neurones in each of our ChAc cases.

Qualitative observations and laminar pathology

To analyse the pathoarchitectonic differences between control individuals and patients, we included one 61 year-old female HD case (CAG-repeat 41) and the complete brain of a 60 year-old female from the Würzburg brain collection [25]. These cases were processed in the same manner as the ChAc cases. The cytoarchitectonic parcellation of the human brain is still a matter of debate. von Economo and Koskinas [21] described five structural types ranging from agranular (Type 1) to granulous (Type 5). They included TE1 and TE2 into the so-called frontal type (Type 2), a type of isocortex spread over the rostral two-thirds of the frontal lobe, the superior parietal lobule, including the dome of the postcentral gyrus, the anterior insular gyri and the middle (T2) and inferior (T3) temporal gyri. Therefore, we have selected this type of iscortex to document widespread late-stage HD pathoarchitectonic changes in a type of cortex that can be unequivocally located and identified macroscopically in the human brain. This type of cortex is also considered as a representative of polymodal association cortex engaged in higher cognitive functions and widely connected to other polymodal association cortices of the parietal and occipital lobes.

Photographic work

High-power photographs were obtained using a Canon EOS 5D MKII camera equipped with a Canon MP-E65 macro lens. As a rule, the contrast of the digital pictures was enhanced using Adobe Photoshop CS5 (Adobe Systems Incorporated, San Jose, CA, USA).

Immunohistochemistry

The medial temporal gyrus close to the plane of section depicted in Figure 1c was cut out from parallel unstained 420 μm thick sections, embedded in paraffin and cut with a section thickness of 12 μm. Immunohistochemical detection of glial fibrillary acidic protein (GFAP) was performed with a Ventana Benchmark (Roche Diagnostics (Schweiz) AG, Rotkreuz) autostainer using the SuperVision 2 polymer system (DCS PD000 kit; Innovative Diagnostik-Systeme GmbH & Co., Hamburg, Germany). HD tissue embedded in paraffin and cut at 12 μm thickness tended to float-off even from gelatin-coated or sialylated coverslips during the immunohistochemical procedures. Therefore, we have stained excess slides with a silver impregnation protocol [36].

Statistical analyses

We performed a one-way analysis of variance (Kruskal–Wallis *H*-test) to investigate whether the medians of the ages at death or the medians of estimated cortical neuronal numbers differed between controls, ChAc, and/or HD patients. Rank analysis of variance was followed by posthoc multiple comparisons with and without adjusted *P*-values (BiAS for Windows, Version 9.14; Epsilon, Darmstadt, Germany). *P*-values ≤ 0.05 were considered statistically significant.

Results

The weight of the unfixed brains varied considerably (Table 2). Four of the five HD cases had lower brain weights than the age- and gender-matched control cases ($P = 0.04$). In contrast, the brain weights of the ChAc cases widely overlapped with those of the controls ($P = 0.66$).

As shown in Table 2, the cortical volumes of our HD cases were always lower than those of the controls, and of two of the three ChAc cases. The cortical volumes of the ChAc cases also varied widely and there was no correlation between brain weight and cortical volume. All ChAc cases had a lower cortical neurone density than the HD or control cases (Table 2).

Total neurone number was calculated by multiplying neuronal density and total cortical volume. The total neurone number of our ChAc cases was lower than that of the five control cases ($P = 0.03$), and below that of the majority of our HD cases, although this difference was not statistically significant ($P = 0.64$).

The human cerebral cortex is composed of a high number of diversified cytoarchitectonic fields. We selected the von Economo-Koskinas area TE1, which corresponds to Brodmann's areas 21 and 22, to document pathoarchitectonic differences between the controls and the brains with chorea. TE1, a polymodal association cortex of the human telencephalon, exhibited a clear-cut, six-layered horizontal design that lined the dorsal and ventral walls of most of the superior temporal sulcus in the control cases (Figures 1a and 2b). Further characteristic features were prominent IIIc pyramidal cells, the presence of a layer IV, and wide infragranular layers with prominent layers Va and b. Abundant small-calibre fibres that emanated from the central medullary ray and pierced the cortex (radial fibres, Figures 1a and 2a black asterisks) added vertical striation to the horizontal isocortical architecture. The central medullary ray of the control cases appeared homogeneous, compact and only slightly stained.

In the late stages of HD, conspicuous laminar neuronal loss in layers IIIb/c, V and VI was pathognomonic (Figures 1b and 2c). Cortical thickness was reduced and neurone loss rendered an overall pallor to the affected layers. Superficial layer V pyramidal cells and layer IV granule cells normally interdigitate, blurring the border between layers IV and V (Figures 1a and 2b). In HD, the majority of the superficial layer V pyramidal cells were preserved, and the small superficial layer Va pyramidal cells and layer IV granule cells formed a highly characteristic cell-rich band, which was flanked by pale layers III and Vb (Figures 1b and 2c). Vertical striation was inconspicuous at low magnification. However, higher magnification revealed numerous thin, pale, densely packed radial fibres traversing the infragranular layers V and VI in HD. Also, the central medullary ray was shrunken, chromophilic (i.e. intensely stained with gallocyanin), and separated from the atrophic layer VI by a pale rim. These features characterized the late stages of HD and facilitated diagnosis of stained thick sections using the naked eye.

In contrast with the late stages of HD, laminar pathology appeared less compelling in the late stages of ChAc (Figure 2a,d). However, closer examination revealed that the IIIc pyramidal cells were almost completely lost in all isocortical regions (Figure 2c; white

arrow) and the thickness of the combined layers Va and IV appeared to be reduced, with a high cellular density; this was similar to the corresponding layers in HD cases. In ChAc1 and ChAc2, where there was a shorter time interval between clinical diagnosis and death, we found extended (ChAc2) or restricted (ChAc1) isocortical regions, with an evidently unimpaired layer IIIc. A considerable diffuse increase in the number of mainly astroglial cells increased the overall staining of layers III and V, where neuronal loss appeared less evident (Figure 2a,d). This increased density of predominantly reactive astrocytes complicated the cell counting process in ChAc cases and increased the time required. Vertical striation and the diameters of individual radial fibres were more marked in these patients than in the control or HD cases. In general, the contours of the radial fibres appeared blurred, even though they were taken within the focus range of the macroscopic photo lens. The central medullary ray was not chromophilic. Nevertheless, it appeared less homogenous and compact than the control central medullary ray (Figure 2b,d).

Regions showing astrogliosis (positive GFAP immunoreactivity) were mainly confined to the subcortical white matter and deep cortical layers VI and V in ChAc3 (Figure 3a). In this case, there was an obvious mismatch between immunohistochemical GFAP positivity and the increased density of astrocytes in the supragranular layers. Numerous small round and faintly stained nuclei of astrocytes blurred the laminar boundaries in superficial layers (Figure 2d), whereas focal GFAP-positive clusters were observed after immunostaining (Figure 3c). Only weak astrogliosis was identified by GFAP immunoreactivity in the 61 year-old female HD case (Figure 3d). After silver impregnation, astrocytic fibres and some astrocytes were identified in the medullary and deep cortical (Figure 3e) and the superficial cortical layers (Figure 3f). However, the Gallyas silver stain is capricious and the results varied due to methodological variables such as the duration of impregnation.

Discussion

ChAc and HD share common clinical features together with progressive striatal neurodegeneration whereas cortical nerve cell loss was considered absent or mild in ChAc [5–16]. To our knowledge, design-based stereological studies on differences in cortical neurone number in both diseases have not been performed so far.

Cortical neurone loss in ChAc

The mean cortical neurone loss of 46% in our three genetically confirmed ChAc cases compared with the control group ($P = 0.03$; Table 1) seemed surprisingly high. It was also higher than the mean 33% cortical neurone loss observed in our HD cases. ChAc3, the case with the longest duration, had the highest brain weight (volume) of all ChAc cases analysed exceeding that of all HD cases investigated and, however, the lowest neuronal density. Consequently, the total cortical neurone number (volume multiplied with neurone density) in this case was 1.4×10^9 (−39%) cells lower compared with HD3, the case with the lowest neurone number of the 5 HD cases investigated. Nevertheless, there was no statistically significant difference between these disease groups ($P = 0.64$). This comparison clearly shows that cerebral volume and neurone density alone are unreliable estimators of cortical integrity, total neurone number, and the rate of neurodegeneration. Furthermore, the impact

of a low sample number and a high biological variation in human data must always be taken into account. A reverse condition could be observed in terminal stages of HD, which were characterized by a high cell density and low cortical volume (Figure 2b,c and figure 3.2 in Rüb *et al.* [37]).

Our results on cortical neurone loss are at odds with the majority of previous neuropathological reports relating to ChAc. Several reasons may explain this discrepancy. ChAc is a rare disease, and few post-mortem studies of the central nervous system have been published to date [5–16]. The majority of these authors found either no, or only mild to moderate, cortical pathology. However, the clinical diagnosis in the majority of previously published cases was not verified genetically, even though a relevant review considered it likely that most of the published cases were *VPS13A* mutation-positive [38]. Ishida [13] reported an increased density of GFAP-positive cells in the cerebral cortex without significant neurone loss, in a case with autosomal recessive *VPS13A* mutation [39]. Miki *et al.*[14] found asymmetric neurone loss in area 4, with bilateral pyramidal tract degeneration in the spinal cord and an absence of gliosis or neurone loss in the temporal lobe in a case with heterozygous mutations in exon 32 (c.3419_3420 delCA) and exon 35(c.3970_3973 delAGTC) of the *VPS13A* gene. This patient suffered from generalized tonic-clonic seizures and died at age 47, 12 years after diagnosis of the first clinical symptoms. Connolly *et al.* [15] reported a reduced density of parvalbumin-positive interneurones in the middle frontal, parietal and superior temporal lobes in two siblings with genetically confirmed ChAc. Rafalowska *et al.* [10] described hypocellularity in lamina III of the frontal cortex, differently oriented pyramidal cells, and very large neurones in a familial case of ChAc. Their male patient without genetic testing was acanthocytes-positive (34–43% acanthocytes in the blood); acanthocytes were demonstrable to a lesser extent in the blood of his mother. Mente *et al.* noted a right-sided hippocampal atrophy with neuronal loss and gliosis in hippocampal fields CA1, CA3 and CA4, possible granule cell dispersion, sparing of CA2 and the subiculum, and unremarkable cerebral hemispheres including temporal neocortex in their case with a brain weight of 1550 g [16]. Unfortunately, neither of these authors applied advanced stereological protocols on serially cut and stained hemispheres to estimate global cortical neurone loss. Local neurodegeneration in the motor cortex and hippocampal fields could result from side effects of epileptic seizures, reduced neurone density of parvalbumin neurones from inherent reduced staining intensities after immunohistochemical procedures or highly divergent individual shrinkage factors, and, finally, disoriented pyramidal cells from additional intrauterine or postnatal neurodevelopmental disorders.

Pathoarchitectonics

The minor change in the overall brain weights observed in the majority of ChAc cases investigated to date, the presence of unimpaired myelinated radial fibres (see figure 1c,f in [14]), and absence of circumscribed laminar cell loss as observed in HD could have suggested an intact cortical architecture and could explain the underestimation of neuronal death in ChAc by previous and recent investigators. The widespread IIIc pyramidal cell degeneration and layer V and VI neurone loss in the polymodal association cortices of all cerebral lobes in our ChAc cases was masked by a massive astrogliosis. This contrasts with our late-stage HD cases. In this stage, layer-specific neurone loss resulted in pallor of

gallocyanin-stained sections, a pathognomonic horizontal striation and a characteristic neurone loss in allorcortical regions [37,40].

Axons of IIIc pyramidal cells and their collaterals contribute substantially to the overall number of myelinated fibres in the central medullary ray of cortical gyri [41]. Atrophy and basophilia of the subcortical medulla in gallocyanin-stained sections were additional features of advanced HD stages. Furthermore, we observed a high density of pale and thin radial fibres, which connected the cortex and the central medullary ray. The peripheries of the central medullary rays in HD assume a brush-like appearance in thick sections; these appear to be decorated by numerous brittle branches. Our gallocyanin stained sections provided no information related to the number, origin, termination, and unilateral or reciprocal connections of the axons within an individual radial fibre. Finally, we have no data on the total number of radial fibres. Their high density, which reflects neuronal loss and closer spacing, may erroneously suggest the complete resistance of radial fibres in terminal stages of HD. Researchers who do not take into account the impact of brain shrinkage, may misinterpret high fibre and neurone density as simple atrophy instead of a decreased total number of remaining neurones and fibres in regions with heavy neurodegeneration.

Viewed superficially, cortical pathology in ChAc seems less compelling. Further studies will be required to investigate why the cortical neurone loss in ChAc is associated with radial fibre hypertrophy and spares most of the cortical volume and central medullary ray morphology. Diffuse astrogliosis could fill the gaps left by degenerating neuronal perikarya and processes. This would be in line with dense GFAP-positive immunostaining of the central medullary ray and the infragranular cortical layers V and VI. Striking diffuse astrogliosis in gallocyanin stained sections could explain the blurred contours of the radial fibres in low power magnification. The apparent mismatch between focal GFAP positivity in the supragranular layers and diffuse astrogliosis in gallocyanin stained sections in ChAc and different staining results with GFAP and Gallyas silver impregnation for astroglia in the central medullary ray of HD need additional investigation in well-controlled cases with short post-mortem intervals and different fixation protocols. A possible impact of reactive neurite sprouting from surviving neurones remains to be verified in additional cases of ChAc.

Alternatively, a complete (vertical) loss of minicolumns [42,43] in ChAc *vs.* a layer-specific horizontal neurone loss in HD could also explain the observed pathoarchitectonic differences between HD and ChAc. In this regard, ChAc would be a neurodegenerative disease characterized by hypertrophy of the peripheral neuropil space of cortical minicolumns. Minicolumn assessment could complement diagnostic and functional considerations. Minicolumns were wider and with more neuropil space in two cases with dyslexia [44] and in an age-dependent manner in cases with autism [45] and schizophrenia [46], whereas smaller minicolumns have been described in older cases with autism [47,48], in Asperger syndrome [49], Alzheimer's disease [50], and ageing [51].

Clinicopathological correlations

Dementia Our sample consisted of three ChAc cases spanning a wide period between clinical diagnosis and death. Therefore, any generalizations or sophisticated clinicopathological correlations must be interpreted with caution. All of our ChAc or HD

patients developed dementia during the later stages of the disease. Widespread IIIc pyramidal cell loss in polymodal association cortices could represent a morphological substrate of dementia in different neurodegenerative diseases including Alzheimer's disease, Pick's disease, virus-induced dementia, chorea Huntington [19] and ChAc. In the initial stage of the disease, all of our five HD cases were characterized clinically by psychiatric symptoms, mood disturbances, and behavioural problems before the onset of choreatic movements [19]. This deteriorating clinical symptomology could be explained by heterogenous cortical neurone and interneurone loss during disease progression [52,53]. We observed several regions with intact groups of layer IIIc pyramidal cells in each cerebral lobe of ChAc1 and 2. However, the number of ChAc cases examined was too low to permit quantitative immunohistochemical studies of interneurones. Gliosis and the impact of cortical folding, particularly in coronal section planes, hindered the analysis of subregions with less IIIc pyramidal cell degeneration.

Chorea HD and ChAc share chorea as a central clinical feature. Nearly 100 years ago, the Vogts postulated a combined role for cortical and striatal pathology in the aetiology of movement disorders and cognitive deficits [54] although striatal neurodegeneration was initially considered the leading cause of movement disorders and subcortical dementia. Mayeux *et al.* [55] criticize this concept as misleading. Indeed, besides the neuronal loss in layers III, Vb and VI, our ChAc cases were characterized by striatal neurone loss, which exceeded that of our HD cases [18]. Furthermore, there is evidence for an early cortical involvement in HD [37] and it is still a matter of debate whether neurodegeneration of cortico-striatal axons is causing dysfunction and degeneration of striatal neurones in an anterograde manner [56,57] or retrograde and transneuronal pathways from the striatum and thalamus can induce cortical neurodegeneration. Shepherd [58] discusses the yet unresolved role of intratelencephalic and pyramidal tract neurones and their disconnection in the pathophysiology of HD. Our observation of pyramidal cell loss in layers III and Va and b in HD and ChAc lend support to this concept.

Concluding remarks

Given that our HD cases without genetic confirmation were not confounded with other rare diseases mimicking clinical Chorea Huntington, we conclude that HD and ChAc are associated with similar levels of neuronal loss, while other cortical neuropathological features differ. From a molecular biological point of view, HD pathogenesis is driven by a toxic gain of function whereas ChAc is characterized by a loss of function. Cortical atrophy, relative gliosis, and degeneration are hallmarks of late HD cases whereas a marked proliferation of astroglia apparently preserves macroscopic features and masks cortical neurone loss in ChAc. Both diseases could be considered as a kind of 'natural experiment' to study the different role of astroglia in neurodegenerative diseases with similar clinical symptoms Uncovering selective vulnerability at the system level in both diseases is of paramount importance in order to localize the earliest irreversible neuronal death, to understand the selective and disease-specific vulnerability of particular cells or cell layers, and ultimately to identify how the progression of pathological features associated with neurodegenerative diseases can be halted.

Acknowledgements

We thank the patients and their families for their willingness to donate brain tissue for research. The Advocacy for Neuroacanthocytosis Patients (www.naadvocacy.org), founded by the late Glenn Irvine and his family, contributed with great enthusiasm whenever there was a need to help out financially or otherwise. We thank Hans Jung, Valerio Saglini and Johannes Haybäck for collaboration.

Funding

This work was supported by the ERA-net E-Rare consortium EMINA (European Multidisciplinary Initiative on Neuroacanthocytosis; BMBF 01GM1003) and by the National Natural Science Foundation of China (Grant No. 81601099); Deutsche Huntington-Hilfe e.V. and Huntington-Selbsthilfe NRW e.V. (to U.R.); Drs. Hans and Elisabeth Feith-Foundation (Huntington disease research; to U.R.); the Scientific Research Foundation for the Returned Overseas Chinese Scholars, State Education Ministry [(2015) No. 1098]; Beijing Talents Fund (2015000026833ZK06); Beijing Municipal Administration of Hospitals Youth Program (QML20150801); Support Project of High-level Teachers in Beijing Municipal Universities in the Period of 13th Five-year Plan (CIT&TCD201804091); Clinical-Basic Medicine Cooperation Fund of Capital Medical University (16JL28).

References

1. Walker RH, Saiki S, Danek A. Neuroacanthocytosis syndromes II. Berlin Heidelberg: Springer, 2008
2. Rampoldi L, Dobson-Stone C, Rubio JP, Danek A, Chalmers RM, Wood NW, Verellen C, Ferrer X, Malandrini A, Fabrizi GM, Brown R, Vance J, Pericak-Vance M, Rudolf G, Carre S, Alonso E, Manfredi M, Nemeth AH, Monaco AP. A conserved sorting-associated protein is mutant in chorea-acanthocytosis. Nat Genet 2001; 28: 119–20 [PubMed: 11381253]
3. Dobson-Stone C, Danek A, Rampoldi L, Hardie RJ, Chalmers RM, Wood NW, Bohlega S, Dotti MT, Federico A, Shizuka M, Tanaka M, Watanabe M, Ikeda Y, Brin M, Goldfarb LG, Karp BI, Mohiddin S, Fananapazir L, Storch A, Fryer AE, Maddison P, Sibon I, Trevisol-Bittencourt PC, Singer C, Caballero IR, Aasly JO, Schmierer K, Dengler R, Hiersemenzel LP, Zeviani M, Meiner V, Lossos A, Johnson S, Mercado FC, Sorrentino G, Dupre N, Rouleau GA, Volkmann J, Arpa J, Lees A, Geraud G, Chouinard S, Nemeth A, Monaco AP. Mutational spectrum of the CHAC gene in patients with chorea-acanthocytosis. Eur J Hum Genet 2002; 10: 773–81 [PubMed: 12404112]
4. Ueno S, Maruki Y, Nakamura M, Tomemori Y, Kamae K, Tanabe H, Yamashita Y, Matsuda S, Kaneko S, Sano A. The gene encoding a newly discovered protein, chorein, is mutated in chorea-acanthocytosis. Nat Genet 2001; 28: 121–2 [PubMed: 11381254]
5. Bird TD, Cederbaum S, Valey RW, Stahl WL. Familial degeneration of the basal ganglia with acanthocytosis: a clinical, neuropathological, and neurochemical study. Ann Neurol 1978; 3: 253–8 [PubMed: 666266]
6. Iwata M, Fuse S, Sakuta M, Toyokura Y. Neuropathological study of chorea-acanthocytosis. Jpn J Med 1984; 23: 118–22 [PubMed: 6727056]
7. Alonso ME, Teixeira F, Jimenez G, Escobar A. Chorea-acanthocytosis: report of a family and neuropathological study of two cases. Can J Neurol Sci 1989; 16: 426–31 [PubMed: 2804805]
8. Hardie RJ, Pullon HW, Harding AE, Owen JS, Pires M, Daniels GL, Imai Y, Misra VP, King RH, Jacobs JM. Neuroacanthocytosis. A clinical, haematological and pathological study of 19 cases. Brain 1991; 114: 13–49 [PubMed: 1998879]
9. Rinne JO, Daniel SE, Scaravilli F, Pires M, Harding AE, Marsden CD. The neuropathological features of neuroacanthocytosis. Mov Disord 1994; 9: 297–304 [PubMed: 8041370]
10. Rafalowska J, Drac H, Jamrozik Z. Neuroacanthocytosis. Review of literature and case report. Folia Neuropathol 1996; 34: 178–83 [PubMed: 9812420]
11. Vital A, Bouillot S, Burbaud P, Ferrer X, Vital C. Chorea-acanthocytosis: neuropathology of brain and peripheral nerve. Clin Neuropathol 2002; 21: 77–81 [PubMed: 12005256]
12. Bader B, Arzberger T, Heinsen H, Dobston-Stone C, Kretzschmar H, Danek A Neuropathology of chorea-acanthocytosis In Neuroacanthocytosis Syndromes II. Eds Walker RH, Saiki S, Danek A. Berlin Heidelberg: Springer, 2008; 187–95

13. Ishida C, Makifuchi T, Saiki S, Hirose G, Yamada M. A neuropathological study of autosomal-dominant chorea-acanthocytosis with a mutation of VPS13A. Acta Neuropathol 2009; 117: 85–94 [PubMed: 18584183]
14. Miki Y, Nishie M, Ichiba M, Nakamura M, Mori F, Ogawa M, Kaimori M, Sano A, Wakabayashi K. Chorea-acanthocytosis with upper motor neuron degeneration and 3419_3420 delCA and 3970_3973 delAGTC VPS13A mutations. Acta Neuropathol 2010; 119: 271–3 [PubMed: 19949804]
15. Connolly BS, Hazrati LN, Lang AE. Neuropathological findings in chorea-acanthocytosis: new insights into mechanisms underlying parkinsonism and seizures. Acta Neuropathol 2014; 127: 613–15 [PubMed: 24394886]
16. Mente K, Kim SA, Grunseich C, Hefti MM, Crary JF, Danek A, Karp BI, Walker RH. Hippocampal sclerosis and mesial temporal lobe epilepsy in chorea-acanthocytosis: a case with clinical, pathologic and genetic evaluation. Neuropathol Appl Neurobiol 2017; 43: 542–6 [PubMed: 28398599]
17. Jellinger KA. Neurodegenerative disorders with extrapyramidal features – a neuropathological overview. J Neural Transm Suppl 1995; 46: 33–57 [PubMed: 8821040]
18. Liu J, Heinsen H, Grinberg LT, Alho E, Amaro E Jr, Pasqualucci CA, Rüb U, den Dunnen W, Arzberger T, Schmitz C, Kiessling M, Bader B, Danek A. Subcortical neurodegeneration in chorea: more differences than similarities between chorea-acanthocytosis and Huntington's disease. Parkinsonism Relat Disord 2018; 49: 54–9 [PubMed: 29402698]
19. Heinsen H, Strik M, Bauer M, Luther K, Ulmar G, Gangnus D, Jungkunz G, Eisenmenger W, Götz M. Cortical and striatal neurone number in Huntington's disease. Acta Neuropathol 1994; 88: 320–33 [PubMed: 7839825]
20. Brodmann K Vergleichende Lokalisationslehre der Großhirnrinde. Leipzig: Barth, 1909
21. von Economo C, Koskinas GN. Die Cytoarchitekonik der Hirnrinde des erwachsenen Menschen. Wien Berlin: Julius Springer, 1925
22. Seidel K, Siswanto S, Brunt ERP, den Dunnen W, Korf HW, Rüb U. Brain pathology of spinocerebellar ataxias. Acta Neuropathol 2012; 124: 1–21 [PubMed: 22684686]
23. Rolfs A, Koeppen AH, Bauer I, Bauer P, Buhlmann S, Topka H, Schols L, Riess O. Clinical features and neuropathology of autosomal dominant spinocerebellar ataxia (SCA17). Ann Neurol 2003; 54: 367–75 [PubMed: 12953269]
24. Margolis RL, Holmes SE, Rosenblatt A, Gourley L, O'Hearn E, Ross CA, Seltzer WK, Walker RH, Ashizawa T, Rasmussen A, Hayden M, Almqvist EW, Harris J, Fahn S, Macdonald ME, Mysore J, Shimohata T, Tsuji S, Potter N, Nakaso K, Adachi Y, Nakashima K, Bird T, Krause A, Greenstein P. Huntington's disease-like 2 (HDL2) in North America and Japan. Ann Neurol 2004; 56: 670–4 [PubMed: 15468075]
25. Heinsen H, Arzberger T, Schmitz C. Celloidin mounting (embedding without infiltration) – a new, simple and reliable method for producing serial sections of high thickness through complete human brains and its application to stereological and immunohistochemical investigations. J Chem Neuroanat 2000; 20: 49–59 [PubMed: 11074343]
26. Heinsen H, Heinsen YL. Serial thick, frozen, gallocyanin stained sections of human central nervous system. J Histotechnol 1991; 14: 167–73
27. Kreczmanski P, Heinsen H, Mantua V, Woltersdorf F, Masson T, Ulfig N, Schmidt-Kastner R, Korr H, Steinbusch HWM, Hof PR, Schmitz C. Volume, neuron density and total neuron number in five subcortical regions in schizophrenia. Brain 2007; 130: 678–92 [PubMed: 17303593]
28. West MJ, Slomianka L, Gundersen HJG. Unbiased stereological estimation of the total number of neurons in the subdivisions of the rat hippocampus using the optical fractionator. Anat Rec 1991; 231: 482–97 [PubMed: 1793176]
29. Schmitz C, Eastwood BS, Tappan SJ, Glaser JR, Peterson DA, Hof PR. Current automated 3D cell detection methods are not a suitable replacement for manual stereologic cell counting. Front Neuroanat 2014; 8: 27 [PubMed: 24847213]
30. von Economo C Cellular structure of the human cerebral cortex. Basel: Karger, 2009
31. Schmitz C Towards more readily comprehensible procedures in disector stereology. J Neurocytol 1997; 26: 707–10 [PubMed: 9368883]

32. Schmitz C Variation of fractionator estimates and its prediction. Anat Embryol 1998; 198: 371–97 [PubMed: 9801058]
33. Schmitz C, Rüb U, Korr H, Heinsen H. Nerve cell loss in the thalamic mediodorsal nucleus in Huntington's disease. II. Optimization of a stereological estimation procedure. Acta Neuropathol 1999; 97: 623–8 [PubMed: 10378381]
34. Schmitz C, Hof PR. Recommendations for straightforward and rigorous methods of counting neurons based on a computer simulation approach. J Chem Neuroanat 2000; 20: 93–114 [PubMed: 11074347]
35. Steinbusch HWM, Hof PR, Schmitz C. Neurostereology in the Journal of Chemical Neuroanatomy – conclusion. J Chem Neuroanat 2000; 20: 127. [PubMed: 11074349]
36. Gallyas F An argyrophil III method for the demonstration of fibrous neuroglia. Acta Morphol Acad Sci Hung 1981; 29: 185–93 [PubMed: 6172011]
37. Rüb U, Vonsattel JP, Heinsen H, Korf HW. The neuropathology of Huntington's disease (HD): classical findings, recent developments and correlation to functional neuroanatomy. Adv Anat Embryol Cell Biol 2015; 217: 1–146 [PubMed: 26767207]
38. Danek A, Jung HH, Melone MAB, Rampoldi L, Broccoli V, Walker RH. Neuroacanthocytosis: new developments in a neglected group of dementing disorders. J Neurol Sci 2005; 229–230: 171–86
39. Walker RH, Velayos-Baeza A, Bader B, Danek A, Saiki S. Mutation in the CHAC gene in a family of autosomal dominant chorea-acanthocytosis. Neurology 2012; 79: 198–9; author reply 9
40. Braak H, Braak E. Allocortical involvement in Huntington's disease. Neuropathol Appl Neurobiol 1992; 18: 539–47 [PubMed: 1488086]
41. Morrison JH, Hof PR. Selective vulnerability of corticocortical and hippocampal circuits in aging and Alzheimer's disease. Prog Brain Res 2002; 136: 467–86 [PubMed: 12143403]
42. Buxhoeveden DP, Casanova MF. The minicolumn hypothesis in neuroscience. Brain 2002; 125: 935–51 [PubMed: 11960884]
43. DeFelipe J, Markram H, Rockland KS. The neocortical column. Front Neuroanat 2012; 6: 22 [PubMed: 22745629]
44. Casanova MF, Buxhoeveden DP, Cohen M, Switala AE, Roy EL. Minicolumnar pathology in dyslexia. Ann Neurol 2002; 52: 108–10 [PubMed: 12112057]
45. McKavanagh R, Buckley E, Chance SA. Wider minicolumns in autism: a neural basis for altered processing? Brain 2015; 138: 2034–45 [PubMed: 25935724]
46. Di Rosa E, Crow TJ, Walker MA, Black G, Chance SA. Reduced neuron density, enlarged minicolumn spacing and altered ageing effects in fusiform cortex in schizophrenia. Psychiatry Res 2009; 166: 102–15 [PubMed: 19250686]
47. Casanova MF, van Kooten IAJ, Switala AE, van Engeland H, Heinsen H, Steinbusch HWM, Hof PR, Trippe J, Stone J, Schmitz C. Minicolumnar abnormalities in autism. Acta Neuropathol 2006; 112: 287–303 [PubMed: 16819561]
48. Casanova MF, Buxhoeveden DP, Switala AE, Roy E. Minicolumnar pathology in autism. Neurology 2002; 58: 428–32 [PubMed: 11839843]
49. Casanova MF, Buxhoeveden DP, Switala AE, Roy E. Asperger's syndrome and cortical neuropathology. J Child Neurol 2002; 17: 142–5 [PubMed: 11952076]
50. Buldyrev SV, Cruz L, Gomez-Isla T, Gomez-Tortosa E, Havlin S, Le R, Stanley HE, Urbanc B, Hyman BT. Description of microcolumnar ensembles in association cortex and their disruption in Alzheimer and Lewy body dementias. Proc Natl Acad Sci U S A 2000; 97: 5039–43 [PubMed: 10805766]
51. Chance SA, Casanova MF, Switala AE, Crow TJ, Esiri MM. Minicolumn thinning in temporal lobe association cortex but not primary auditory cortex in normal human ageing. Acta Neuropathol 2006; 111: 459–64 [PubMed: 16496164]
52. Nana AL, Kim EH, Thu DC, Oorschot DE, Tippett LJ, Hogg VM, Synek BJ, Roxburgh R, Waldvogel HJ, Faull RL. Widespread heterogeneous neuronal loss across the cerebral cortex in Huntington's disease. J Huntingtons Dis 2014; 3: 45–64 [PubMed: 25062764]

53. Kim EH, Thu DC, Tippett LJ, Oorschot DE, Hogg VM, Roxburgh R, Synek BJ, Waldvogel HJ, Faull RL. Cortical interneuron loss and symptom heterogeneity in Huntington disease. Ann Neurol 2014; 75: 717–27 [PubMed: 24771513]

54. Vogt C, Vogt O. Zur Lehre der Erkrankungen des striären Systems. J Psychol Neurol 1920; 25: 631–846

55. Mayeux R, Stern Y, Herman A, Greenbaum L, Fahn S. Correlates of early disability in Huntington's disease. Ann Neurol 1986; 20: 727–31 [PubMed: 2949692]

56. Sapp E, Penney J, Young A, Aronin N, Vonsattel JP, DiFiglia M. Axonal transport of N-terminal huntingtin suggests early pathology of corticostriatal projections in Huntington disease. J Neuropathol Exp Neurol 1999; 58: 165–73 [PubMed: 10029099]

57. Jackson M, Gentleman S, Lennox G, Ward L, Gray T, Randall K, Morrell K, Lowe J. The cortical neuritic pathology of Huntington's disease. Neuropathol Appl Neurobiol 1995; 21: 18–26 [PubMed: 7770116]

58. Shepherd GM. Corticostriatal connectivity and its role in disease. Nat Rev Neurosci 2013; 14: 278–91 [PubMed: 23511908]

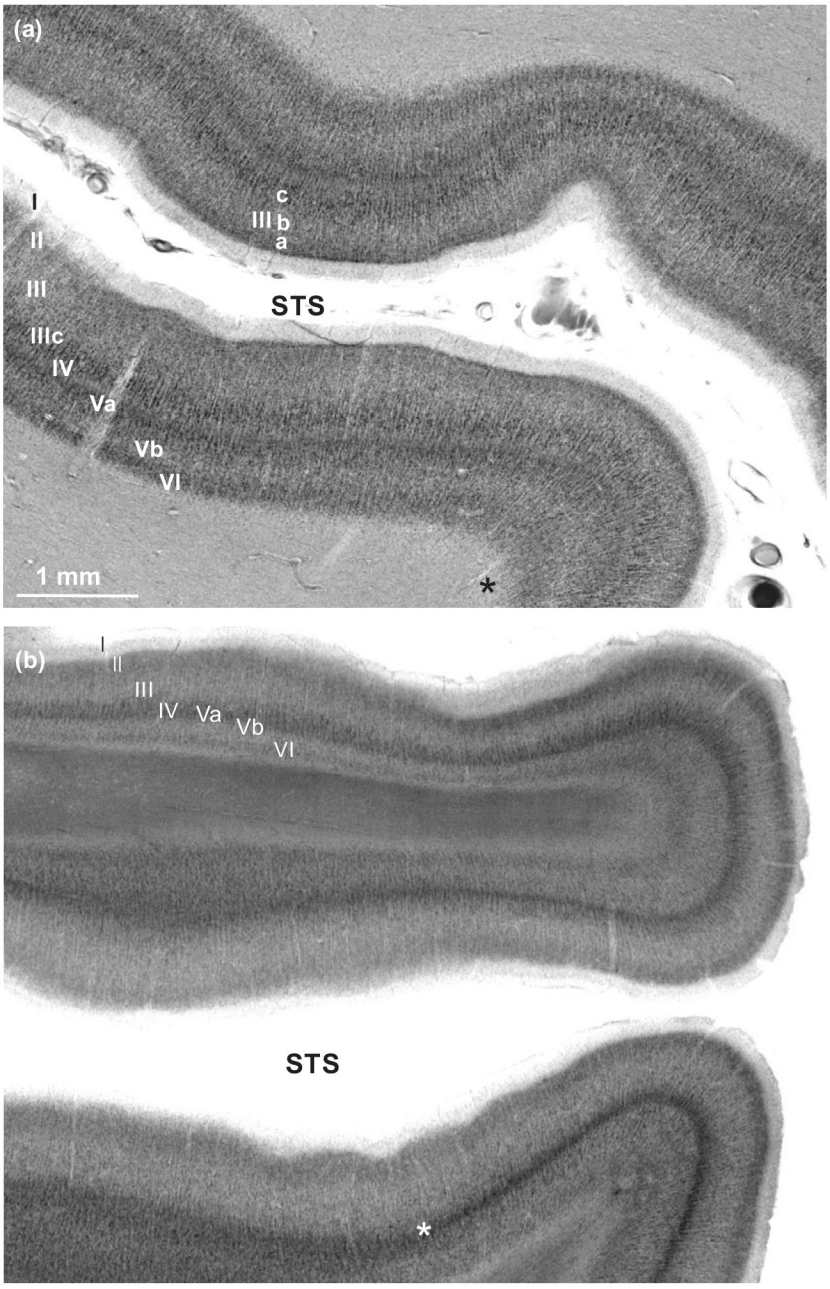

Figure 1.

The dorsal and ventral bank of the superior temporal sulcus (Brodmann's [20] areas 22 and 21; von Economo-Koskinas [21] area temporalis propria or TE1) in gallocyanin stained 420 μm coronal sections. (**a**) 60 year-old female control case. (**b**) 61 year-old female Huntington's disease case. The horizontal layers in this polymodal isocortex are designated with Roman numerals I–VI, and their sublayers with a, b and c. IIIc pyramidal cells are characteristic of polymodal association cortices and can be recognized as small dark spots (see also Figure 2b,c). Note the pallor and thinning of layers III, V and VI, and the hyperchromatic central medullary ray in (**b**). STS superior temporal sulcus. Same magnification in (**a,b**); white asterisk in (**b**): grazing section through combined layers IV and

Va left to and vertical section right to asterisk. Readers interested in studying delicate details of cytoarchitectonics are recommended to open the electronic version of the article and to view the high-resolution PDF images of panels 1 and 2 in Adobe Reader or Acrobat with 200–400% magnification.

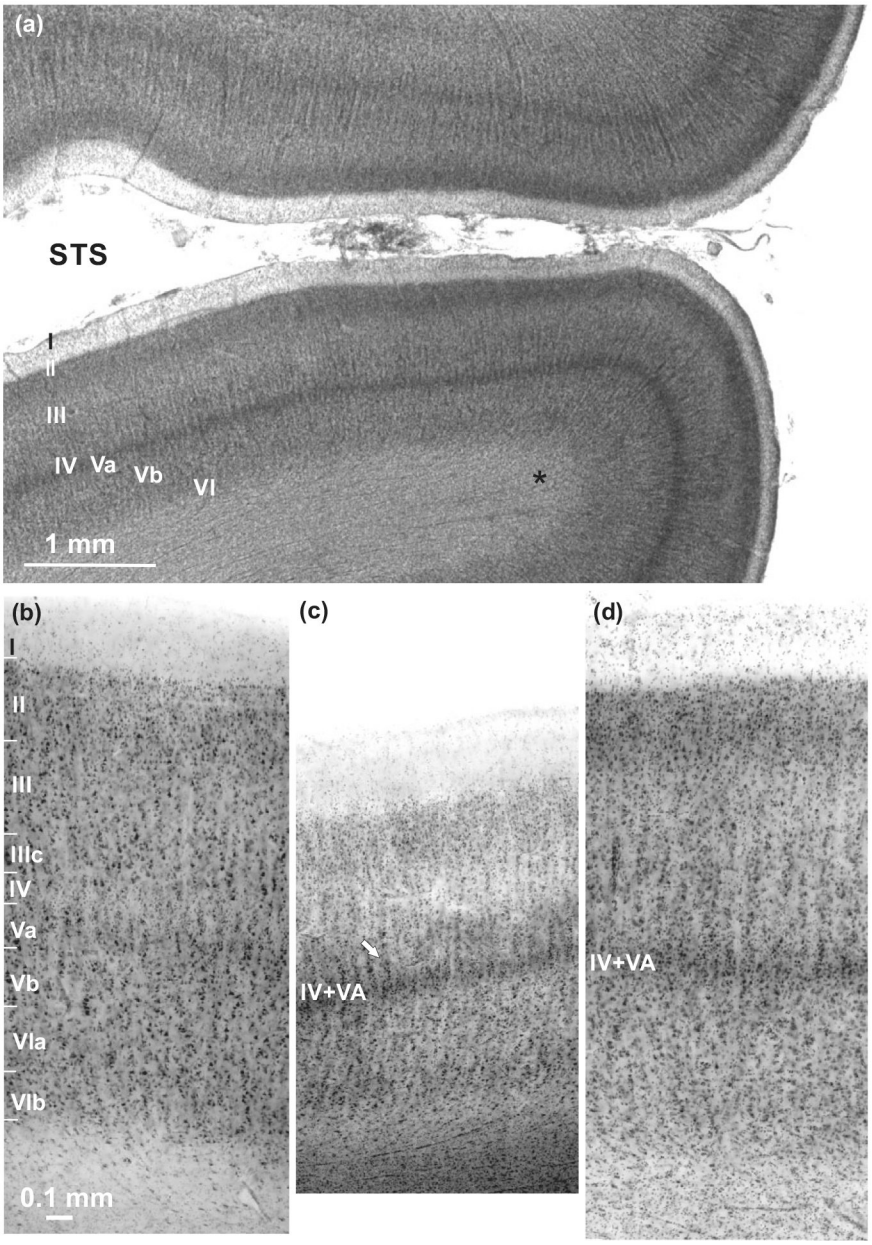

Figure 2.

Low-power macroscopic overview of TE1 of a 54 year-old male chorea-acanthocytosis 3 (ChAc3) case (**a**) and low-power microscopic aspect of area TE1 of the 60 year-old control case (**b**), the 61 year-old Huntington's disease- (HD) (**c**), and the 54 year-old ChAc-case (**d**). Blurred laminar boundaries in cortex with an apparently normal thickness (**a**). The black asterisk in (**a**) indicates unstained fibre bundles that leave the central medullary ray to pierce the cortex in a fan-like manner (radial fibres). The depth of focus of microscopic lenses is less than that of macroscopic photographic lenses and only few cell-sparse radial fibres were within the focus of (**b**) through (**d**). Vertical stacks of pyramidal cells were arranged parallel to the radial fibres and the distance between the parallel neurones gives an impression of the average diameter of radial fibres and the dimensions of minicolumns. Radial fibres or

vertical bundles are an integral part of the minicolumnar peripheral neuropil space [42]. Therefore, the average diameter of minicolumns was obviously higher in ChAc than in the control cases, however, due to cell loss and diffuse astrogliosis the borders were less distinct in ChAc compared with controls. Neurone density was apparently higher in HD (**c**) than in controls (**b**) and ChAc (**d**), however, average neurone size was lower, IIIc pyramidal cells were missing or confined to few radial fibres (arrow), whereas the latter outnumbered those in controls and in ChAc. The average diameter of HD radial fibres was only half or less compared with controls. Bar in (**a**) 100 μm, same magnification in (**b**–**d**). Layers IV and V seemed to be fused in HD and ChAc, and the borders of layers Vb, VIa and VIb were difficult to distinguish in terminal stages of both choreatic diseases.

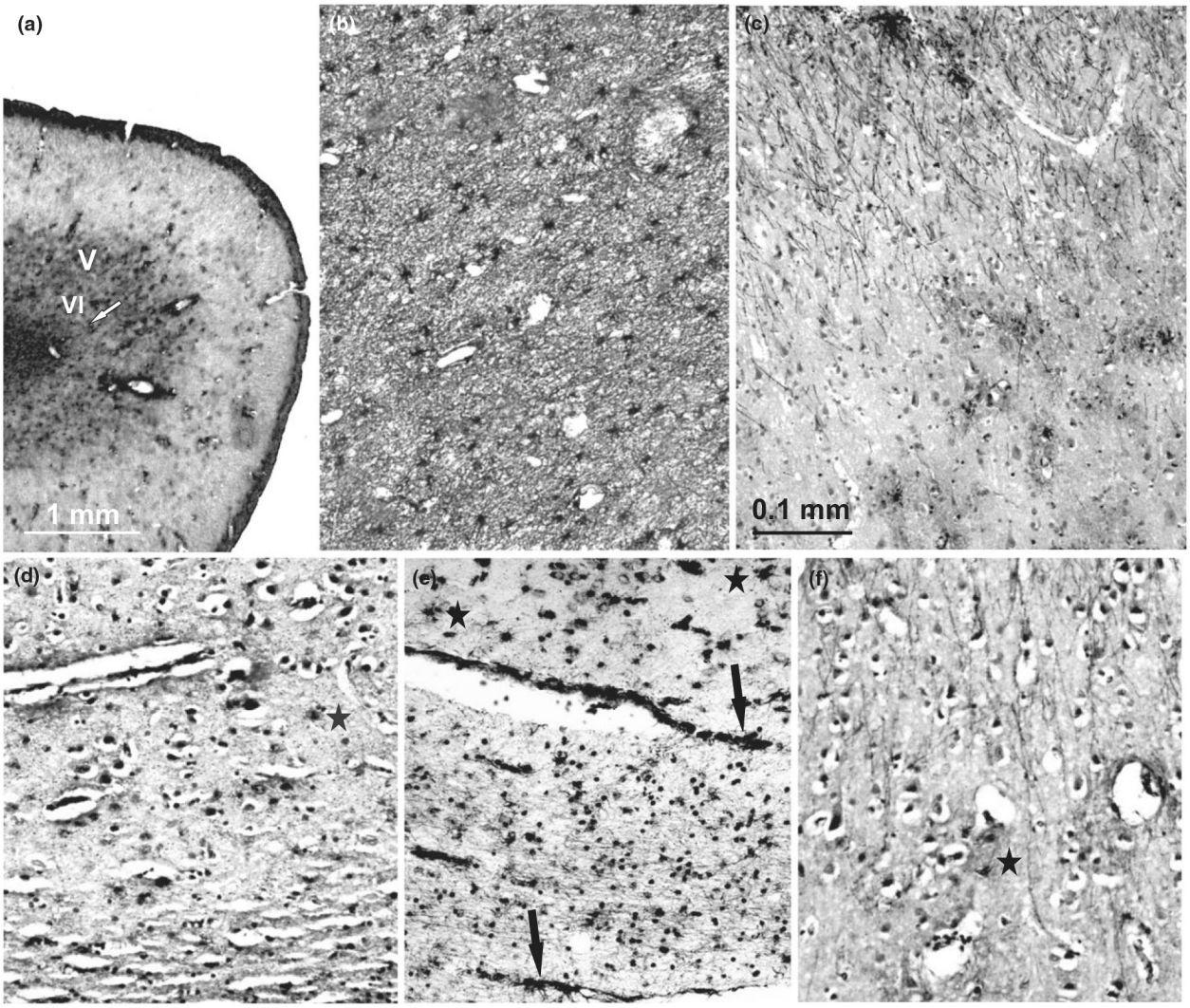

Figure 3.

Astrocytes in the cortex and medullary layer of the medial temporal gyrus in chorea-acanthocytosis (ChAc) (**a**–**c**) and Huntington's disease (HD) (**d**–**f**). (**a**) Glial fibrillary acidic protein (GFAP) immunohistochemistry in ChAc3 shows high signal intensity in the medullary and deep cortical layers (VI and V) (white arrow) and focal intensity in the supragranular layers. (**b**) Higher magnification view displaying a high density of GFAP-positive astrocytic perikarya and a dense meshwork of fibres in the central medullary ray (**b**), hypertrophic astrocytic perikarya and long vertically coursing fibres in the supragranular layers of the medial temporal gyrus (**c**). Autoclaving of paraffin sections for GFAP-immunostaining caused detachment of the sections or considerable artifacts, particularly in the medullary layer (lower part of Figure (**d**) of our HD cases. Silver impregnation with a modified Gallyas staining (**e,f**) showed a loose mesh of long thin astrocytic fibres in the cortical medulla. A dense sleeve of fibres and astrocytic perikarya was only present around bigger vessels at the cortical-subcortical border (**e** black arrows). Few astrocytes were observed in layer VI (**e** black star). After Gallyas impregnation, the supragranular layers of

TE2 (**f**) were characterized by inconspicuous perikarya of astrocytes (black star) and radially oriented long thin fibres. Same magnification in (**c**) through (**e**).

Table 1.

Main demographic and clinical data of the cases investigated

Case	Gender	Age at onset	Age at death	Disease duration	Symptoms	Genetic findings
ChAc 1	M	30	35	5	Chorea, cognitive decline, dysarthria	4428_4431del & 5084 T>A
ChAc 2	F	34	48	14	Chorea, OD, CD, dystonia	c.4592delT & c.4592delT
ChAc 3	M	27	54	27	Chorea, OD, CD, seizures, dystonia, dysarthria, dysphagia, parkinsonism	c.6419C>G & c.9190del
HD 1	F	24	36	12	Chorea, schizophrenia-like psychosis	NA
HD 2	M	29	40	11	Chorea, inability to perform manual skills; suicidal behaviour	NA
HD 3	M	29	41	12	Chorea, alcoholism, promiscuity; manic-depressive episodes, nocturnal aggression, progressive dementia	NA
HD 4	F	36	54	18	Chorea, change of personality, aggressive, paranoid behavior	NA
HD 5	M	65	72	7	Chorea; disturbance of concentration and memory, aggression, paranoid ideation	NA
HD 6	F	35	61	26	Death by starvation; case only used for photographic documentation	CAG-repeat 45
Control 1	M	NA	36	NA	Myocardial infarct	
Control 2	F	NA	46	NA	Accidental CO-intoxication	
Control 3	M	NA	49	NA	Myocardial infarct	
Control 4	F	NA	58	NA	Gastrointestinal bleeding, gastric cancer	
Control 5	M	NA	75	NA	Pulmonary embolia	
Control 6	F	NA	60	NA	Myocardial infarct	

Data of HD 1–HD 5 and control 1–control 5 were from Heinsen *et al.* [19].

CD, cognitive decline; ChAc, chorea-acanthocytosis; HD, Huntington Disease; NA, not available; OD, orofacial dyskinesia.

Neuropathol Appl Neurobiol. Author manuscript; available in PMC 2020 April 01.

Table 2.

Demographic data, quantitative data on brain weight, cortical volume, neuron density, total cortical neuron number, total number of unidentified cortical cells

Gender	Disease duration	Brain weight	Hemisph	Cortical volume (cm^3)	Cortical neuron-density n/mm^3	Cortical neuron-number ($\times 10^9$)	Number of uni-dentified cortical cells ($\times 10^6$)
Chorea-acanthocytosis (ChAc)							
M	5	1320	Right	114	25,810	2,942	579
F	14	1240	Right	144	30,723	4,424	687
M	27	1450	Left	119	19,078	2,270	466
Mean	15	1337	–	126	25,204	3,212	577
	***ChAc vs. HD P > 0.05**	**†ChAc vs. control P > 0.05** **†ChAc vs. HD P > 0.05**		**†ChAc vs. control P > 0.05** **†ChAc vs. HD P > 0.05**		**†ChAc vs. control P = 0.03** **†ChAc vs. HD P > 0.05**	
Huntington's disease (HD)							
F	12	1105	Left	93	42,022	3,911	411
M	11	1266	Left	127	33,075	4,222	669
M	12	1141	Left	103	35,963	3,705	542
F	18	1170	Left	108	38,543	4,199	525
M	7	1200	Left	108	36,135	3,914	721
Mean	12	1176	–	108	37,148	3,990	573
		†HD vs. control P = 0.04		**†HD vs. control P = 0.02**		**†HD vs. control P = 0.03**	
Controls							
M	–	1440	Left	141	41,722	5,918	586
F	–	1470	Left	135	43,997	5,959	596
M	–	1620	Left	150	39,780	5,996	530
F	–	1250	Left	129	42,708	5,548	544
M	–	1250	Left	133	48,291	6,450	767
Mean	–	1406	–	138	43,300	5,974	605

Data of HD 1–HD 5 and control 1–control 5 were from Heinsen *et al.* [19].

**P*-values estimated by Mann–Whitney *U* test.

† *p*-values estimated by multiple Dunn comparisons; corrected according to Bonferroni-Holm.